# Free Energy Surfaces for the α(1 → 4)-Glycosidic Linkage: Implications for Polysaccharide Solution Structure and Dynamics

**Michelle M. Kuttel[†,‡] and Kevin J. Naidoo*[,†,§]**

*Department of Chemistry, University of Cape Town, Cape Town, South Africa, Department of Computer Science, University of Cape Town, Cape Town, South Africa, and Centre for High Performance Computing, Western Cape, South Africa*

*Received: November 17, 2004; In Final Form: February 14, 2005*

We present a potential of mean force surface for rotation about $\phi$ and $\psi$ dihedral angles of the α(1 → 4)-glycosidic linkage in the maltose disaccharide (4-*O*-α-D-glucopyranosyl-D-glucopyranose) in aqueous solution. Comparison of the vacuum and solution free energy surfaces for maltose shows the principal effects of water to be an increase in the rotational freedom of the α(1 → 4) linkage brought about by lowering the energy barrier for syn to anti conformational changes as well as expansion of the range of low-energy $\phi,\psi$ conformations. This free energy analysis thus provides a thermodynamic and conformational rationale for the effects of water on α(1 → 4)-linked polysaccharides and carbohydrate glasses.

## 1. Introduction

Glucose-α(1 → 4)-glucose is the backbone glycosidic linkage in three abundant biological storage polysaccharides: amylose, amylopectin, and glycogen. Experimental and computational investigations have shown that the α(1 → 4)-glycosidic bond in glucans is conformationally restricted.[1−3] Experiments indicate that, when solvated, the maltose (4-*O*-α-D-glucopyranosyl-D-glucopyranose) glycosidic angle conformation shifts from the crystal structure values[4,5] of $\phi,\psi = 5°,13°$ to conformations closer to the $\phi,\psi = -30°,-30°$ region.[6−9] This finding is corroborated by computer simulations.[10−14] Moreover, the presence of water has a dramatic effect on the physical properties of both maltose[15−17] and amylose,[17−22] lowering the sugar glass transition temperature ($T_g$). Dielectric relaxation experiments have shown the strength of the $\beta$-relaxation processes in both glucose and maltose glasses to increase with increasing water content.[23]

Recently, we proposed a novel method for calculating the strengths of intramolecular hydrogen bonds. Our calculations show that an intramolecular hydrogen bond across the α(1 → 4) linkage significantly limits the rotational freedom of the glycosidic bonds in the gas phase.[24] This was, however, not the case in the solution phase, where the intramolecular hydrogen bonds were in competition with the sugar−water intermolecular hydrogen bonds.[25]

Adiabatic Ramachandran maps have been used extensively for predicting the conformational space of disaccharides, where two-dimensional maps of the $\phi$ and $\psi$ dihedral angles are typically calculated.[1,2,13,26,27] However, entropic and solvent contributions to the molecular energy are not incorporated into an adiabatic energy surface. For a saccharide in solution, where the entropic component of the energy can be large, adiabatic maps are likely to give an inadequate approximation of the glycosidic linkage conformational space.

We previously calculated the NMR relaxation carbohydrate parameters in solution for saccharides containing the α(1 → 4)- and α(1 → 6)-glycosidic linkages. The simulated relaxation parameters compared favorably with those produced by NMR experiment.[28,29] The NMR analysis revealed that the α(1 → 4)-glycosidic linkage is not very flexible. However, these simulations and experiments could not establish the extent of the solvent molecules on the conformation of solvated saccharides.

Ideally, free energy calculations are required to provide a complete characterization of the conformational space available to a carbohydrate in solution. A carbohydrate potential of mean force in solution incorporates energetic contributions from the conformational enthalpy and entropy of the carbohydrate, the configurational entropy of the solvent, and solvent−solute interactions. Potential of mean force calculations allow for identification of the number of low-energy conformers, the flexibility of each conformer, the time spent in each conformation, and the rate of conversion between conformers.

Both maltose and the similar dixylose disaccharide (4-*O*-α-D-xylopyranosyl-α-D-xylopyranose) have previously been investigated with partial potential of mean force calculations.[10,30] However, both calculated surfaces were restricted to a central $\phi,\psi$ region encompassing a minimum conformation as surmised from NMR and crystallography data. A complete surface was not possible because of sampling difficulties and the significant computational cycles demanded by potential of mean force (PMF) calculations. Here, we calculate a complete PMF surface for rotation about the $\phi,\psi$ glycosidic dihedral angles of maltose in aqueous solution. This is compared with the vacuum free energy surface calculated previously[31] to identify the thermodynamic effects of water on the α(1 → 4)-glycosidic linkage. In addition, one-dimensional minimum path potential of mean force trajectories derived from the solution and vacuum PMFs for maltose are shown. These give a clear one-dimensional representation of the relative minima and energy barriers in the $\phi,\psi$ vacuum and solution PMFs. The implications of this analysis for the effect of water on conformation and physical properties of α(1 → 4)-linked glucans are discussed.

* Author to whom correspondence should be addressed. Fax: +27-21-689-7499. E-mail: knaidoo@science.uct.ac.za.
† Department of Chemistry, University of Cape Town.
‡ Department of Computer Science, University of Cape Town.
§ Centre for High Performance Computing.

10.1021/jp044756m CCC: $30.25 
Published on Web 03/30/2005

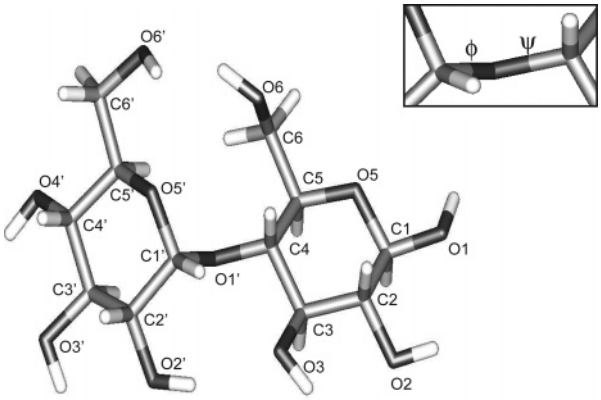


**Figure 1.** Three-dimensional structure of maltose showing the atomic naming convention used. The inset shows the bonds of rotation for the and dihedral angles.

## 2. Computational Methods

The principle degrees of freedom for maltose (Figure 1) are the two torsion angles, $\phi = H_1'-C_1'-O_1-C_4$ and $\psi = C_1'-O_1'-C_4-H_4$ where $C_4$ and $H_4$ are the aglyconic atoms. The definitions for $\phi$ and $\psi$ are analogous to $\phi_H$ and $\psi_H$ in IUPAC convention.

The $\beta$-configuration of the disaccharide was simulated as it is expected to be favored in solution, in accordance with the anomeric ratio for glucose in water.[32−34]

**2.1. Adaptive Umbrella Sampling.** The $\phi,\psi$ potential of mean force (PMF) surface for $\beta$-maltose in explicit aqueous solution was calculated using an iterative adaptive umbrella sampling method.[35−39]

Umbrella sampling simulations use a modified Hamiltonian function, $H$

$$H = H^\circ + U(\bar{\xi}) \tag{1}$$

where $H^\circ$ is the Hamiltonian of the system and $U(\bar{\xi})$ is an applied biasing potential. The aim of the biasing, or "umbrella", potential is to direct the system into unsampled regions. The unperturbed probability density, $P(\bar{\xi})$, for a generalized multidimensional degree of freedom, $\bar{\xi}$, may be obtained from the biased probability density generated by a simulation, $P'(\bar{\xi})$, using the equation

$$P(\bar{\xi}) = CP'(\bar{\xi})\, e^{\beta U(\bar{\xi})} \tag{2}$$

where $C$ is an arbitrary constant and $\beta = -1/kT$. In the iterative *adaptive* umbrella sampling procedure, the aim is to converge on an umbrella potential that will achieve uniform sampling in the entire region of $\bar{\xi}$ during a standard simulation. Successive simulations are run with "adapting" umbrella potentials until a uniform distribution is achieved. The potential of mean force, $W(\bar{\xi})$, can be obtained from the final probability distribution function, $P(\bar{\xi})$, using the relation

$$W(\bar{\xi}) = -kT \ln P(\bar{\xi}) \tag{3}$$

where $k$ is the Boltzmann constant and $T$ is the temperature.

For the maltose simulations, the 360° × 360° umbrella potential surface for the $\phi,\psi$ dihedral angles was represented as a two-dimensional grid of points, with a grid separation of 2.5°. Although a 2.5° × 2.5° grid is computationally expensive, coarser grids were found to provide an inadequate estimate of the disaccharide PMFs, thus hindering conversion of the adaptive umbrella sampling routine. This was particularly the case in the steeper barrier regions of the map. An iterative procedure was used to converge on the $\phi,\psi$ potential of mean force, as follows:

(1) Simulation $i$, of length $N_i$ is performed with an umbrella potential $U_i(\phi,\psi)$ ($U_1(\phi,\psi) = 0$ for all $\phi,\psi$). At each integration step of the simulation, the biasing potential energy corresponding to the current $\phi,\psi$ position is calculated from a cubic spline of the umbrella energy surface.

(2) The biased probability distribution for simulation $i$ is computed as a two-dimensional $\phi,\psi$ distribution histogram by summing the number of configurations in each 2.5° × 2.5° bin over the production phase of the simulation trajectory.

(3) The biased distribution functions, $n_j(\phi,\psi)$, for all simulations $j = 1, 2, ..., i$ are combined using the weighted histogram analysis method (WHAM)[38−42] (with a tolerance value of 0.001) to obtain an optimal estimate for the unbiased distribution function, $P(\phi,\psi)$.

(4) The current potential of mean force estimate, $W_i(\phi,\psi)$, is calculated from $P(\phi,\psi)$ using eq 3.

(5) $W_i(\phi,\psi)$ is extrapolated to as yet unexplored regions by setting the unsampled regions to the maximum value of the umbrella potential.

(6) Any discontinuities in $W_i(\phi,\psi)$ introduced by extrapolation are limited by smoothing the potential map three times in each dimension using the function $U'_{k,l} = {}^1/_3(-0.3U_{k-2,l} + 1.3U_{k-1,l} + U_{k,l} + 1.3U_{k+1,l} - 0.3U_{k+2,l})$.[38]

(7) Regions in the two-dimensional $\phi,\psi$ PMF associated with high-energy steric clashes of the atoms are removed by setting any bin in the PMF with an energy value greater than a predetermined cutoff of 20 kcal/mol to the cutoff value.

(8) The algorithm terminates when convergence is reached. Convergence is defined when, during a single simulation, every bin in $n_j(\phi,\psi)$ in the $\phi,\psi$ range of interest is occupied at least once. If the convergence is not met, then $U_{i+1}(\phi,\psi)$ is set to $-W_i(\phi,\psi)$, $i$ is incremented, and the procedure is returned to step 1.

The first simulation was started from a minimized and equilibrated coordinate set and performed with a flat umbrella potential surface. In each umbrella simulation, an equilibration period of 500 ps was followed by a data collection period used to obtain the $\phi,\psi$ distribution histogram. The data collection phase was in the range of 1−10 ns, to allow for rotational equilibrium of the hydroxymethyl groups.[43] Successive simulations in a series were gradually run for longer periods as the PMF estimates improved and more of the phase space was explored. Approximately 500 ns of simulation time was required to produce each of the final PMF surfaces.

Equilibrium $\phi,\psi$ populations were obtained from the calculated PMF curves using the relation $P = e^{-W/kT}$. In addition, one-dimensional $\psi$ PMFs were calculated from the $\phi,\psi$ PMFs by the following a simple procedure. The population of a particular $\psi$ point was obtained by summing all of the contributing $\phi$ populations. The $\psi$ PMF can then be calculated from the normalized $\psi$ population distribution.

The minimum energy helical conformations predicted by the maltose PMF for an α(1 → 4)-linked oligosaccharide in solution and vacuum were investigated by constructing two maltododecaose molecules with $\phi,\psi$ values corresponding to the global minimum energy syn conformations in a vacuum and solution, respectively. The structures were minimized with the glycosidic linkages constrained to the assigned values, using 500 cycles of "steepest descent" minimization followed by 2000 cycles of "conjugate gradient" minimization. In addition, the average chain conformation for a 300 unit amylose polysac-

charide was estimated by random assignment of the values of $\phi,\psi$ angle pairs in accordance with the population distribution calculated from the maltose solution PMF.

**2.2. Adiabatic Energy Maps.** For comparison purposes, a relaxed adiabatic $\phi,\psi$ map for $\beta$-maltose was calculated on a $5° \times 5°$ grid. At each point in $\phi,\psi$ space, all other degrees of freedom were relaxed by energy minimization. In addition, for each $\phi,\psi$ conformation, clockwise and anticlockwise arrangements of the secondary hydroxyls and three orientations of the primary hydroxyl (tg, gg, or gt) were considered, i.e., six candidate structures were minimized for each grid point. For each analyzed structure, the steepest descent method was used for 500 steps of initial minimization, followed by up to 2000 steps of conjugate gradient minimization.

**2.3. Simulation Conditions.** Non-Boltzmann molecular dynamics simulations were performed using the program CHARMM[44] (version 27b1), with modifications incorporated into the USERE module to implement the two-dimensional adaptive umbrella sampling PMF calculations. The solution simulations for $\beta$-maltose incorporated one disaccharide molecule surrounded by 489 TIP3P water molecules[45] in a cube of length 24.6433 Å with periodic boundary conditions. This gives a density of 1.013 g/cm$^3$, which is the approximate experimental density of an aqueous maltose solution of this weight percentage (2.2%). The cube was subjected to minimum image periodic boundary conditions to eliminate edge effects. The CSFF parameter set[43] for the CHARMM force field was used for the carbohydrate molecule. CSFF is a modification of a previous carbohydrate parameter set[46] designed to produce experimentally consistent primary and secondary hydroxyl dynamics in solution.

Initial velocities for the atoms were selected at random from a Boltzmann distribution at 300 K. All simulations were performed in the canonical ensemble (constant $n$, $V$, $T$), using stochastic Langevin dynamics with a frictional coefficient of 62.5 to maintain a constant temperature of 300 K. The equations of motion were integrated using a Leapfrog Verlet integrator[47] with a step size of 1 fs. The SHAKE algorithm[48] was used to fix the length of bonds involving hydrogen atoms and the water molecule geometry throughout each simulation. Nonbonded interactions were truncated using a switching function applied on a neutral group basis between 10.0 and 12.0 Å. The groups corresponded to electrically neutral collections of atoms in the carbohydrate molecules and entire water molecules for the solvent.

## 3. Maltose Free Energy Surfaces

Contoured plots of the calculated $\phi,\psi$ adiabatic map and the PMF energy surfaces for $\beta$-maltose are shown in Figure 3. All of the energy surfaces are characterized by two principal low-energy regions (valleys), whose general location is consistent with published adiabatic maps for maltose.[1,2,13,28,49−52] As the $\phi$ angle is considerably more restricted than the $\psi$ angle, these valleys can be defined approximately as $\psi = -20°$ and $\psi = 180°$ (syn and anti conformations respectively). The global minimum is a syn conformation in the case of all three surfaces. Although the adiabatic map global minimum energy conformation at $\phi,\psi = -23.90°,-21.79°$ is close to the vacuum PMF global minimum at $\phi,\psi = -22.5°,-25.0°$, in solution the global minimum shifts to $-47.5°,-35.0°$.

The slight differences apparent between the adiabatic map and vacuum PMF surface can be attributed to the following factors. First, the more exhaustive umbrella sampling procedure is likely to locate minimum energy conformations not discovered by the adiabatic map procedure. This is clearly the case in the areas where the vacuum PMF surface is obviously smoother than the adiabatic map. It also occurs in the $\phi,\psi = -70°,-70°$ region of the map, where a stabilizing $O_3'-O_5$ hydrogen bond was not located by the adiabatic map procedure. Second, the maps will differ where entropy, in the form of molecular flexibility, makes a contribution to the free energy. This appears to occur in both the syn and anti wells, which, though maintaining the same relative energies, are broadened in the vacuum PMF as compared to the adiabatic map.

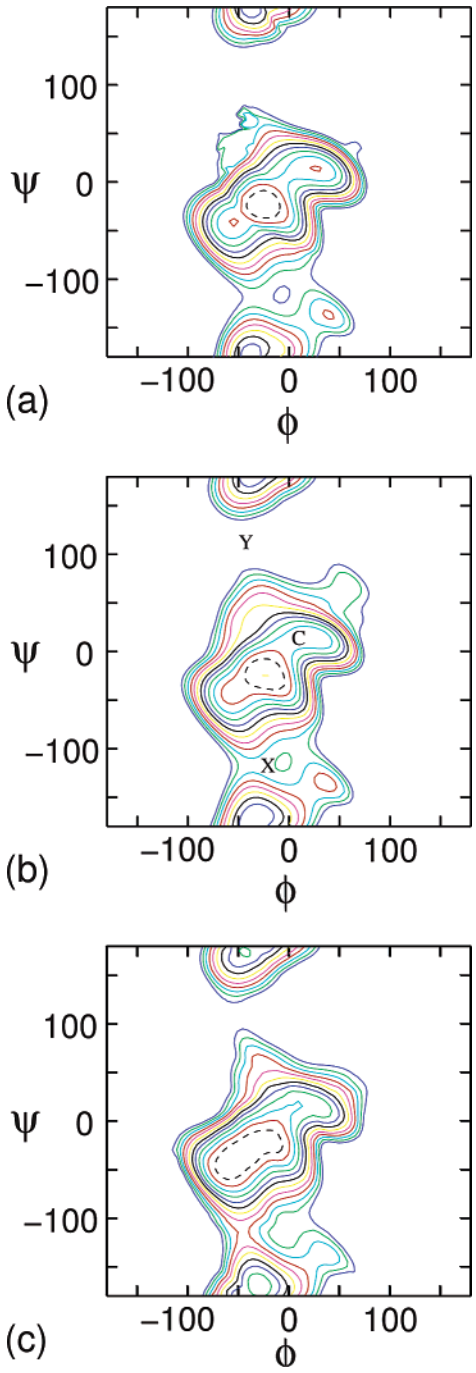


**Figure 2.** Contoured energy surfaces for maltose: (a) adiabatic map, (b) vacuum PMF surface. and (c) PMF surfaces in TIP3P solution. The maltose crystal structure is located in the region indicated by C, and the lowest-energy saddle points of the barriers separating the syn and anti wells are labeled X and Y. Contours are at 1 kcal/mol intervals above the global energy minimum, to a maximum of 12 kcal/mol. The first contour at 1 kcal/mol is dashed.

**3.1. Vacuum Free Energy Surfaces.** In a vacuum, disaccharide conformations can be stabilized by both intraresidue

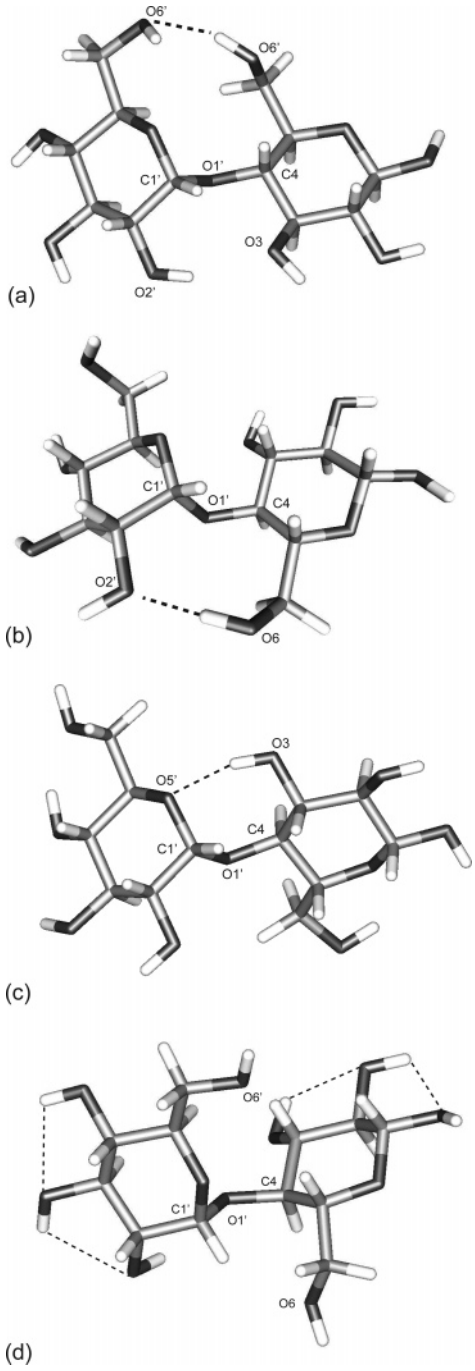


**Figure 3.** Minimum energy configurations for maltose in a vacuum. Stabilizing intramolecular hydrogen bonds are shown with dashed lines: (a) syn conformation, $\phi,\psi = -25°,-25°$; (b) anti conformation, $\phi,\psi = 35°,-170°$; (c) X saddle point conformation, $\phi,\psi = 35°,-115°$; (d) Y barrier conformation, $\phi,\psi = 50°,100°$.

hydrogen bonds involving hydroxyl groups on the same pyranose ring as well as interresidue hydrogen bonds between hydroxyls on different rings. Intraresidue hydrogen bonds around a pyranose ring typically require suboptimal angles for the hydrogen bonds of between 100° and 130°. Therefore, interresidue hydrogen bonds are expected to be more energetically favorable as the hydroxyls are relatively free to align in an ideal configuration. In the syn and anti conformations, both of these types of hydrogen bonds occur, examples of which are shown in Figure 3. In the syn region, two interresidue hydrogen bonds can form simultaneously, one between the $O_2$ and $O'_3$ hydroxyls and the other between $O_6$ and $O'_6$. Distance constraints mean that anti conformations from the $\psi = 180°$ region can

**TABLE 1: Comparison of the Relative Populations at 300 K of the Syn ($\psi \approx 0°$) and Anti ($\psi \approx 180°$) Valley Regions Calculated from the Maltose PMFs**

| | vacuum | solution |
|---|---|---|
| syn region (%) | 99.52 | 98.93 |
| anti region (%) | 0.48 | 1.06 |

**TABLE 2: Approximate Free Energy Differences for Transitions between the Syn and Anti Minima and the X and Y Barrier Regions on the Maltose $\phi,\psi$ Potential of Mean Force Surfaces in a Vacuum and Solution**

| | vacuum | solution |
|---|---|---|
| $\Delta G$ (syn → anti) | 4 | 3 |
| $\Delta G$ (syn → X) | 10 | 8 |
| $\Delta G$ (syn → Y) | 15 | 12 |
| $\Delta G$ (anti → X) | 6 | 6 |
| $\Delta G$ (anti → Y) | 11 | 9 |

form only one interresidue hydrogen bond at a time, which can be either an $O'_2-O_6$ or an $O'_1-O_6$ interaction. The three-centered $O_6-O'_3$ and $O'_3-O_5$ hydrogen bonds seen in large cyclodextrin crystal structures[53,54] and in other adiabatic map calculations[27] did not occur. Both the syn and the anti regions are also entropically favored, as the hydrogen bonds may alternate between the donor and acceptor hydroxyls that have a number of energetically similar configurations. In contrast, the region of the maltose crystal structures (C in Figure 3b), though able to form two interresidue hydrogen bonds, is disfavored by conformational entropy, as was found for the partial maltose vacuum PMF calculated by Brady and co-workers.[37]

Although glycosidic bond rotations via the X and Y barriers both involve some degree of steric clash between atoms, maltose conformations from the saddle point at X can be stabilized by a single intraresidue hydrogen bond between $O'_5$ and $O_3$ (Figure 3c). In conformations corresponding to the Y barrier (Figure 3d), steric clashes between the nonreducing ring and the bulky hydroxymethyl group on the reducing ring prohibit a similar bond between $O'_5$ and $O_6$. In addition, steric clashes also prevent the $O_6$ hydroxyl from forming any stabilizing intramolecular hydrogen bonds, such as an $O_6-O_5$ interaction. These interactions account for the energetic difference between the X and Y barriers (~5 kcal/mol, Table 2). Thus, transition between the syn and anti minima in a vacuum is expected to occur chiefly via the saddle point at X.

**3.2. Effects of Water.** Aqueous solvation affects both the relative energies of the two minimum energy wells and barrier heights between them. The energy difference between the syn and anti wells is lowered by approximately 1 kcal/mol (Table 2), with the result that the population of anti ($\psi = 180°$) conformers doubles in solution as compared to vacuum (Table 1). Moreover, the heights of the X and Y barriers are lowered, with the result that transition between the syn and anti minima becomes more probable in aqueous solution. This can be clearly seen in the vacuum and solution minimum energy profiles for rotation about the $\psi$ angle, shown in Figure 5b. One-dimensional PMFs for the $\psi$ dihedral (Figure 5c) were calculated from the two-dimensional PMF populations in a vacuum and solution. These show very similar profiles to the $\psi$ minimum energy paths in Figure 5b. However, the barriers to rotation are lower in the $\psi$ PMF because the entire population of a particular $\psi$ value is taken into account.

A further effect of the water solvent is to broaden and extend the syn well toward more negative $\phi,\psi$ values, away from the C conformation. This change is demonstrated by the $\psi$ population histograms for the syn region at 300 K (Figure 4a); the solution histogram is broader with a median at $\psi = -35°$, in

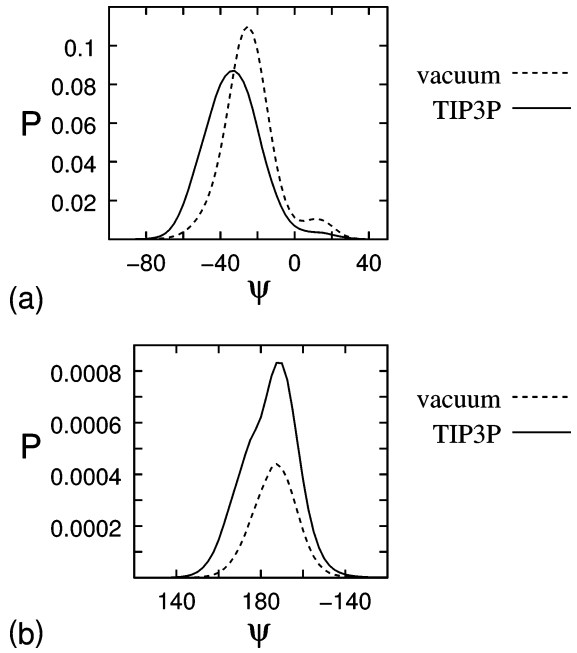


**Figure 4.** Normalized equilibrium populations of the maltose $\psi$ dihedral in a vacuum and solution at 300 K in (a) the syn conformation and (b) the anti conformation.

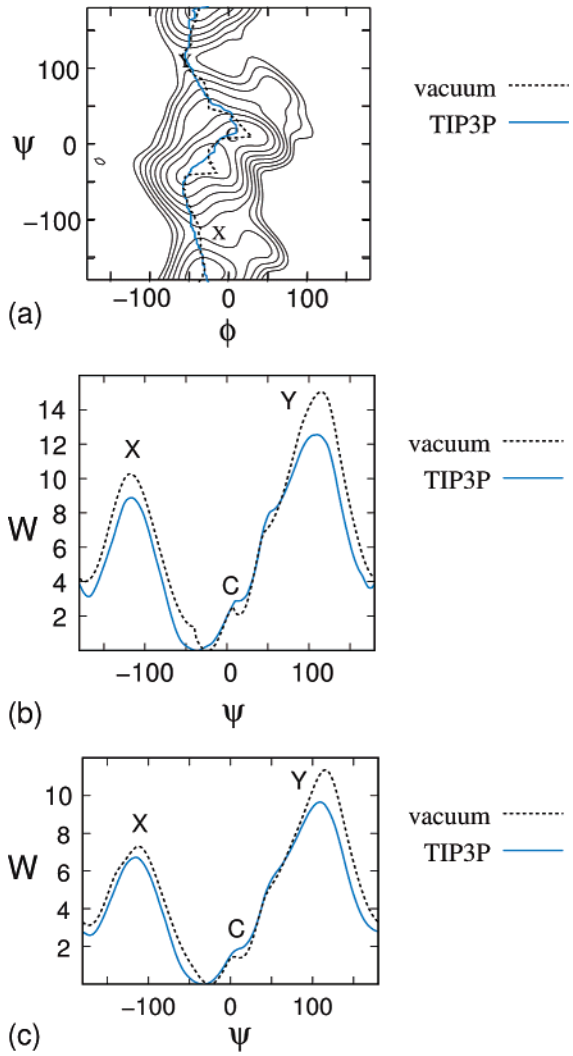


**Figure 5.** (a) Vacuum and solution maltose minimum energy paths for rotation about the glycosidic linkage superimposed on the maltose solution PMF surface. (b) Corresponding minimum energy profiles in a vacuum and solution for the $\psi$ dihedral angle from obtained from the $\phi,\psi$ PMFs. (c) PMF profiles for rotation about the $\psi$ dihedral in maltose in a vacuum and solution obtained from the $\phi,\psi$ populations. The profiles are shown relative to their global energy minima, with the energy in kcal/mol. Regions corresponding to X and Y barriers on the $\phi,\psi$ maps are labeled. The syn and anti conformations correspond to $\psi \approx -20°$ and $\psi \approx -170°$, respectively.

contrast to the solution value of $\psi = -25°$. This is consistent with various experimental[6,7,9,55] and molecular dynamics simulation studies,[12,13,56] which found similar shifts in the maltose $\phi,\psi$ populations upon solvation.

The broadening of energy wells in the solution PMF is due to the water molecules providing alternative hydrogen-bonding partners for the maltose hydroxyl groups. We have previously calculated, using a combination of density functional B3LYP/6-31G(d) quantum methods and classical molecular dynamics simulations, the energetic difference between intramolecular hydroxyl−hydroxyl hydrogen bonds and intermolecular hydroxyl−water hydrogen bonds to be in the region of 1 kcal/mol.[25] The presence of water thus reduces the enthalpic advantage of the vacuum intramolecular and, particularly, interresidue hydrogen bonds. Favorable interactions between the solution and solute molecules also have the effect of lowering the relative energy of maltose conformations that are unable to form interresidue hydrogen bonds. As the syn and C well configurations are stabilized with two intraresidue hydrogen bonds compared to one in both the anti well and X saddle point and none for the Y saddle point, the addition of water as a solvent results in a change in the relative energies of these regions. This has the result that the syn well broadens toward conformations that have a greater separation of the primary alcohols. In addition, the syn well becomes shallower in solution relative to the anti well as well as the X and Y saddle points (Table 2). This explains why the energy required for a anti → X transition is unaffected by solvation, whereas the anti → Y barrier is lowered. As discussed earlier, the anti and X regions have approximately the same potential to form internal hydrogen bonds and are therefore affected similarly by solution. However, the Y conformation can form relatively few intermolecular hydrogen-bonding interactions, and therefore transitions across this barrier gain the greatest energetic advantage in solution. This translates to an increase in energy in the absence of water of 2 kcal/mol for the syn well and 1 kcal/mol for the anti X regions relative to the Y barrier.

**3.3. Implications for Polysaccharides.** The increase in the flexibility and range of motion for the α(1 → 4) linkage in maltose provides an explanation for the effect of water on the glass transition temperature; $T_g$ lowering of maltose glasses in the presence of water can be explained not only by disruption of the hydrogen bond network between maltose molecules[16] but also by the increased mobility of maltose. In addition, the flattening of the maltose PMF in solution and the change in the relative energy of the minima has implications for the structure and dynamics of α(1 → 4)-linked oligo- and polysaccharides; by increasing the range of motion of the glycosidic linkage, solvation should result in a more flexible oligosaccharide chain, with a wider range of low-energy conformations.

The backbone glycosidic linkages comprise the principal degrees of freedom in a polysaccharide. Hence, typical structures of α(1 → 4)-linked polysaccharides in solution and vacuum may be inferred from the maltose PMFs. If the glycosidic linkages function independently of each other, then $\phi,\psi$ PMFs calculated for the corresponding disaccharide(s) are sufficient to establish the average conformations and dynamics for oligo- and polysaccharide chains. However, even if successive linkages are not

completely independent (as is likely to be the case), the dimer PMFs should nevertheless still provide valuable insight into the structural and dynamic properties of the polysaccharides.

Amylose, one of the two polymeric components of starch, consists exclusively of α(1 → 4) linkages. Despite being one of the first carbohydrates to be investigated, the conformation of amylose in different environments has not yet been satisfactorily determined. Amylose forms various flexible helical structures in the solid state.[57−59] A variety of theoretical and experimental studies have suggested two possible structures for amylose in a neutral aqueous solution, either a random coil[60−63] or an "interrupted helix".[64] The interrupted helix structure is suggested to comprise a combination of loose, helical sections, each containing about 100 glucose units, which alternate with short, flexible, random coil segments.[64] When amylose is moved from dimethylsulfoxide to an aqueous solution, a conformational change has been proposed to occur from a well-formed regular helix to a random coil that reflects changes in the torsion angles of the glycosidic linkages.[63,65]

There has been some debate on the nature of the helical twist in the solid state forms of amylose.[66] Conformations taken from the C well, which is the region of the maltose crystal structure, generate right-handed helices. However, this region was found to be less populated compared with other syn conformations in both vacuum and solution cases. Syn conformations of the glycosidic linkages result in left-handed helical conformations of the amylose polysaccharide in a vacuum and solution. Therefore, unless packing effects dramatically alter the preferred conformations of the glycosidic linkage, amylose by extension is likely to form left-handed helices in the solid state. Polysaccharide conformations corresponding to the global minimum energy conformations in a vacuum have 7 glucose units per helical turn and a helical pitch of about 14 Å, compared to a helical turn of about 5.5 units and a helical pitch of around 15 Å for the solution conformation. Thus, in water the shift of the global minimum in the maltose PMF into more negative $\phi,\psi$ regions results in a more slender and extended helical structure for an oligosaccharide. In addition, the broadening of the syn valley upon aqueous solvation implies that α(1 → 4)-linked oligosaccharide helices will become more flexible and disordered in solution, with a broader range of low-energy helical conformations. However, assumptions of the structure of amylose polysaccharides should not be made on the basis of the syn valley alone—all of the low-energy conformations of the glycosidic linkage must be considered. The impact of anti conformations are of particular interest. Because of their low incidence, these conformations are not likely to have a pronounced effect on the properties of maltose and have been largely ignored in modeling studies of α(1 → 4)-linked oligomers.[56] However, if the maltose solution populations are extrapolated to large polymers, 1% of the glycosidic linkages will be in an anti conformation. These conformations, termed "band-flips", have been recently shown to occur in large cyclomaltooligosaccharides, where they are associated with kinks in the strand that are thought to reduce steric strain.[53,59] Figure 6 displays an example of the conformation of a 300 unit amylose strand produced from a random assignment of torsion angle values in accordance with the population distribution for maltose in solution. This tertiary structure consists of straight helical sections interspersed with nonhelical bend regions and is in agreement with the "interrupted helix" proposed for amylose in solution.[64] Here we propose that the bends are not simply random coil regions but are each associated with an anti conformation of a dihedral angle. The bends disrupt the helical

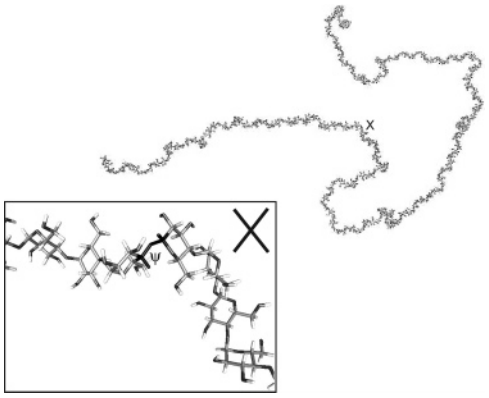


**Figure 6.** Example of a conformation for a 300 unit amylose strand in solution, based on a random assignment of $\phi,\psi$ angles in agreement with populations calculated from the maltose solution PMF surface. Inset shows enlargement at point X. The indicated dihedral angle is in the anti conformation.

predisposition of the syn conformations, rotating the helix by roughly 90°. A similarly constructed conformation based on the maltose vacuum PMF (not shown) has more regular and compact helical conformations, with fewer anti conformation bend regions. Thus, comparison of the vacuum with the solution structure supports the suggested transition of amylose from an interrupted helical conformation in water to a more compact helix in dimethylsulfoxide.[63] However, because anti conformations result in large bends, steric crowding from neighboring molecules in a glassy or crystalline solid state could result in lower anti populations than is the case in solution or vacuum.

## 4. Conclusions

We here presented the first solution PMF for maltose that covers all of the phase space. These PMFs allowed for a quantitative analysis of the effects of water on the α(1 → 4) linkage. Aqueous solvation was shown to expand the range of low-energy structures in maltose, lower the transition barriers between the two minima, and thus flatten the PMF surface compared with the vacuum case. In addition, the relative energies of the syn and anti minima are altered, such that anti conformations of the α(1 → 4) linkage are likely to be more prevalent in solution than previously thought. On the basis of these calculations for maltose, we propose that the tertiary structure of the α(1 → 4)-linked amylose polysaccharide comprises left-handed helical regions interrupted by bends associated with anti conformations.

**Acknowledgment.** M.K. thanks the National Research Foundation (NRF, Pretoria, South Africa) and the University of Cape Town for doctoral support. K.J.N. thanks the United States Department of Agriculture (USDA) for support (USDA-ARS grant no. 58-4012-5-F120).

## References and Notes

(1) Ha, S. N.; Madsen, L. J.; Brady, J. W. *Biopolymers* **1988**, *27*, 1927−1952.
(2) French, A. D. *Carbohydr. Res.* **1989**, *188*, 206−211.
(3) Brant, D. A.; Liu, H.-S.; Zhu, Z. S. *Carbohydr. Res.* **1995**, *278*, 11−26.
(4) Quigley, G. J.; Sarko, A.; Marchessault, R. H. *J. Am. Chem. Soc.* **1970**, *92*, 5834−5839.
(5) Gress, M. E.; Jeffrey, G. A. *Acta Crystallogr., Sect. B: Struct. Sci.* **1977**, *33*, 2490−2495.
(6) Shashkov, A. S.; Lipkind, G. M.; Kochetkov, N. K. *Carbohydr. Res.* **1986**, *147*, 175−182.
(7) Rees, D. A.; Thorn, D. *J. Chem. Soc., Perkin Trans. 2* **1977**, 191−201.

(8) Lipkind, G. M.; Verovsky, V. E.; Kochetkov, N. K. *Carbohydr. Res.* **1984**, *133*, 1−13.
(9) Stevens, E. S.; Sathyanarayana, B. K. *J. Am. Chem. Soc.* **1989**, *111*, 4149−4154.
(10) Ha, S. N.; Giammona, A.; Field, M.; Brady, J. W. *Carbohydr. Res.* **1988**, *180*, 207−221.
(11) Glennon, T. M.; Zheng, Y.; le Grand, S. M.; Shutzberg, B. A.; Merz, K. M. J. *J. Comput. Chem.* **1994**, *15*, 1019−1040.
(12) Ott, K.; Meyer, B. *Carbohydr. Res.* **1996**, *281*, 11−34.
(13) Naidoo, K. J.; Kuttel, M. *J. Comput. Chem.* **2001**, *22*, 445−456.
(14) Tvaroška, I.; Carver, J. P. *J. Phys. Chem. B* **1997**, *101*, 2992−2999.
(15) Miller, D. P.; de Paulo, J. J. *J. Phys. Chem. B* **2000**, *104*, 8876−8883.
(16) van den Dries, I. J.; van Dusschoten, D.; Hemminga, M. A. *J. Phys. Chem. B* **1998**, *102*, 10483−10489.
(17) Lourdin, D.; Ring, S. G.; Colonna, P. *Carbohydr. Res.* **1998**, *306*, 551−558.
(18) Doane, W. L. *Starch*/*Staerke* **1992**, *44*, 293−295.
(19) Kirby, A. R.; Clark, S. A.; Parker, R.; Smith, A. C. *J. Mater. Sci.* **1993**, *28*, 5937−5942.
(20) Liu, Q.; Thompson, D. B. *Carbohydr. Res.* **1998**, *314*, 221−235.
(21) Hulleman, S. H. D.; Janssen, F. H. P.; Feil, H. *Polymer* **1998**, *39*, 2043−2048.
(22) Stading, A.; Rindlav-Westling, A.; Gatenholm, P. *Carbohydr. Polym.* **2001**, *45*, 209−217.
(23) Noel, T. R.; Parker, R.; Ring, S. G. *Carbohydr. Res.* **1996**, *282*, 193−206.
(24) Chen, Y.-J.; Naidoo, K. J. *J. Phys. Chem. B* **2003**, *107*, 9558−9566.
(25) Naidoo, K. J.; Chen, Y.-J. *Mol. Phys.* **2003**, *101*, 2687−2694.
(26) French, A. D.; Kelterer, A.-M.; Johnson, G. P.; Dowd, M. K.; Cramer, C. J. *J. Mol. Graphics Modell.* **2000**, *18*, 95−107.
(27) Mendonca, S.; Johnson, G. P.; French, A. D.; Laine, R. A. *J. Phys. Chem. A* **2002**, *106*, 4115−4124.
(28) Best, R. B.; Jackson, G. E.; Naidoo, K. J. *J. Phys. Chem. B* **2001**, *105*, 4742−4751.
(29) Best, R. B.; Jackson, G. E.; Naidoo, K. J. *Spectrosc. Lett.* **2002**, *35*, 625−632.
(30) Naidoo, K. J.; Brady, J. W. *J. Am. Chem. Soc.* **1999**, *121*, 2244−2252.
(31) Kuttel, M.; Naidoo, K. J. *J. Am. Chem. Soc.* **2005**, *127*, 12−13.
(32) Edward, J. T. *Chem. Ind* **1955**, 1102−1104.
(33) Angyal, S. J. *Aust. J. Chem.* **1968**, *21*, 2737−2746.
(34) Angyal, S. J. *Angew. Chem., Int. Ed. Engl.* **1969**, *8*, 157−226.
(35) Hooft, R. W. W.; van Eijck, B. P.; Kroon, J. *J. Chem. Phys* **1992**, *97*, 6690−6694.
(36) Boczko, E. M.; Brooks, C. L. *J. Phys. Chem.* **1993**, *97*, 4509−4513.
(37) Schmidt, R. K.; Teo, B.; Brady, J. W. *J. Phys. Chem* **1995**, *99*, 11339−11343.
(38) Bartels, C.; Karplus, M. *J. Comput. Chem.* **1997**, *18*, 1450−1462.
(39) Bartels, C.; Karplus, M. *J. Phys. Chem.* **1998**, *102*, 865−880.
(40) Kumar, S.; Bouzida, D.; Swendsen, R. H.; Kollman, P. A.; Rosenberg, J. M. *J. Comput. Chem.* **1992**, *13*, 1011−1021.
(41) Kumar, S.; Rosenberg, J. M.; Bouzida, D.; Swendsen, R. H.; Kollman, P. A. *J. Comput. Chem.* **1995**, *16*, 1339−1350.
(42) Kumar, S.; Payne, P. W.; Vãsquez, M. *J. Comput. Chem.* **1996**, *17*, 1269−1275.
(43) Kuttel, M.; Brady, J. W.; Naidoo, K. J. *J. Comput. Chem.* **2002**, *23*, 1236−1243.
(44) Brooks, B. R.; Bruccoleri, R. E.; Olafson, B. D.; States, D. J.; Swaminathan, S.; Karplus, M. *J. Comput. Chem.* **1983**, *4*, 187−217.
(45) Jorgensen, W. L.; Chandrasekhar, J.; Madura, J. D.; Impey, R. W.; Klein, M. L. *J. Chem. Phys* **1983**, *79*, 926−935.
(46) Palma, R.; Himmel, M. E.; Liang, G.; Brady, J. W. Molecular Mechanics Studies of Cellulases. In *Glycosyl Hydrolases for Biomass Conversion*; ACS Symposium Series 769; Himmel, M. E., Ed.; American Chemical Society: Washington, DC, 2001.
(47) Hockney, R. W. *Methods Comput. Phys.* **1970**, *9*, 136−211.
(48) Ryckaert, J. P.; Ciccotti, G.; Berendsen, H. J. C. *J. Comput. Phys.* **1977**, *23*, 327−341.
(49) Fringant, C.; Tvaroška, I.; Mazeau, K.; Rinaudo, M.; Desbrieres, J. *Carbohydr. Res.* **1995**, *278*, 27−41.
(50) Brant, D. A. *Pure Appl. Chem.* **1997**, *69*, 1885−1892.
(51) Stortz, C. A. *Carbohydr. Res.* **1999**, *322*, 77−86.
(52) Mikros, E.; Labrinidus, G.; Pérez, S. *J. Carbohydr. Chem.* **2000**, *19*, 1319−1349.
(53) Jacob, J.; Geβler, K.; Hoffman, D.; Sanbe, H.; Koizumi, K.; Smith, S. M.; Takaha, T.; Saenger, W. *Angew. Chem., Int. Ed.* **1998**, *37*, 606−609.
(54) Jacob, J.; Geβler, K.; Hoffman, D.; Sanbe, H.; Koizumi, K.; Smith, S. M.; Takaha, T.; Saenger, W. *Carbohydr. Res.* **1999**, *322*, 228−246.
(55) Rees, D. A. *J. Chem. Soc. B* **1970**, 877−887.
(56) Shimada, J.; Kaneko, H.; Takada, T.; Kitamura, S.; Kajiwara, K. *J. Phys. Chem. B* **2000**, *104*, 2136−2147.
(57) Hindrichs, W.; Büttner, G.; Steifa, M.; Betzel, C.; Zabel, V.; Pfannemüler, B.; Saenger, W. *Science* **1987**, *238*, 205−208.
(58) Hindrichs, W.; Saenger, W. *J. Am. Chem. Soc.* **1990**, *112*, 2789−2796.
(59) Gessler, K.; Usón, I.; Takaha, T.; Krauss, N.; Smith, S. M.; Okada, S.; Sheldrick, G. M.; Saenger, W. *Proc. Natl. Acad. Sci. U.S.A.* **1999**, *96*, 4246−4251.
(60) Banks, W.; Greenwood, C. T. *Carbohydr. Res.* **1968**, *7*, 414−420.
(61) Brant, D. A.; Dimpfl, W. L. *Macromolecules* **1970**, *3*, 655−665.
(62) Banks, W.; Greenwood, C. T. *Polymer* **1971**, *12*, 141−145.
(63) Cheetham, N. W. H.; Tao, L. *Carbohydr. Polym.* **1998**, *35*, 287−295.
(64) St-Jacques, M.; Sundararajan, P. R.; Taylor, K. J.; Marchessault, R. H. *J. Am. Chem. Soc.* **1976**, *98*, 4386-4391.
(65) Dais, P. *Carbohydr. Res.* **1987**, *160*, 73−93.
(66) Stephen, A. M.; Zobel, H. F. Starch: Structure, Analysis and Application. In *Food Polysaccharides and Their Applications*; Stephen, A. M., Ed.; Food Science and Technology 67; Marcel Dekker: New York, 1995.